Characterization and Application of Nanomaterials 2025, 8(2), 11021.
https://doi.org/10.24294/can11021

Article

Tracking the thermostimulated transformations of silicon suboxide film through absorption edge characterization

Mykola Sopinskyy*, Ivan Indutnyi, Katerina Michailovska, Volodymyr Yukhymchuk

V. Lashkaryov Institute of Semiconductor Physics, National Academy of Sciences of Ukraine, Kyiv 03028, Ukraine
*** Corresponding author:** Mykola Sopinskyy, sopinskyy@ua.fm, sopinsky@isp.kiev.ua

CITATION

Sopinskyy M, Indutnyi I, Michailovska K, Yukhymchuk V. Tracking the thermostimulated transformations of silicon suboxide film through absorption edge characterization. Characterization and Application of Nanomaterials. 2025; 8(2): 11021. https://doi.org/10.24294/can11021

ARTICLE INFO

Received: 23 December 2024
Accepted: 18 March 2025
Available online: 6 May 2025

Abstract: In this work, the structural transformations of a suboxide vacuum-deposited film of $SiO_{1.3}$ composition annealed in an inert atmosphere in a wide temperature range of 100 °C–1100 °C were characterized by the reflection-transmission spectroscopy technique. The experimental spectroscopic data were used to obtain the spectra of the absorption coefficient $\alpha(h\nu)$ in the absorption edge region of the film. Based on their processing, the dependences of Urbach energy E_U and optical (Tauc) bandgap E_o on the annealing temperature were obtained. An assessment of the electronic band gap (mobility gap) E_g was also carried out. Analysis of these dependences allowed us to trace dynamics of thermally stimulated disproportionation of the suboxide film and the features of the formation of nanocomposites consisting of amorphous and/or crystalline silicon nanoparticles in an oxide matrix.

Keywords: non-stoichiometric silicon oxide; SiO_x; nanocomposite; silicon nanoparticles; absorption edge; optical band gap; electronic band gap; mobility gap; Urbach energy

1. Introduction

Silicon suboxide (SiO_x, $x < 2$) films have been the subject of intensive research for several decades. At an early stage, these studies were mainly driven by the widespread use of such films as passive, insulating, and anti-reflective coatings [1,2]. In recent years, non-stoichiometric silicon oxides, both amorphous and crystalline, have attracted increasing attention for both scientific and technological reasons [3–5]. One of these reasons is that high-temperature phase separation of non-stoichiometric SiO_x films is a key method for the formation of composite structures consisting of nanoscale silicon inclusions (amorphous or crystalline) embedded in a silicon oxide matrix [4–9]. The interest in structures with nanoparticles is due to the unique properties of these structures, which can be radically different from the properties of massive homogeneous materials. And silicon nanostructures are one of the three most convenient building blocks of nanotechnology, along with gold and carbon nanostructures [10]. Silicon oxide—nanosilicon composites are of particular interest [11–16] because of their promising use in modern photonic, optoelectronic, and photovoltaic devices; flash memory devices; as field emission cathodes; etc. that are compatible with the mainstream microelectronics technology.

Furthermore, non-stoichiometric SiO_x films show great potential for applications in nonvolatile resistive random access memory (RRAM, ReRAM) [17,18]. These advanced devices operate by switching between high and low resistance states when a voltage is applied to a metal-insulator-metal (M-I-M) memory cell. The development of RRAM devices based on SiO_x films could potentially lead to the low-cost integration of such cells into chips fabricated using silicon-based complementary

metal-oxide-semiconductor (CMOS) technology. The possibility of using RRAM devices based on SiO_x films as electronic synapses in neuromorphic computing has also been demonstrated [19]. Large variations in the structural topology of SiO_x films with low-energy topological defects provide the structural complexity necessary for the implementation of a new, relatively simple, and reliable method for information encryption, storage, and user identification. This method uses a physical key known as the 'physical unclonable function' [20]. The results of theoretical calculations performed in [20] indicate that SiO_x films with a stoichiometry index of $x \sim 1.3–1.5$ are the most promising in this regard.

A review of the above works allows us to conclude that understanding the structure and properties of silicon suboxide is, on the one hand, a scientific problem of some complexity and, on the other hand, of great practical importance. In this work, the near-edge absorption spectra of vacuum-deposited films of $SiO_{1.3}$ composition, both as-deposited and annealed at temperatures from 100 °C to 1100 °C, are studied in more detail using the reflection-transmission technique and analytical processing of the experimental results. We chose the specific temperature range for annealing the samples because structural transformations occur in non-stoichiometric SiO_x films at these temperatures. Specifically, detailed studies using XRD, HRTEM, Raman, IR, and ESR spectral techniques [21–24] have shown that during low-temperature annealing, the broken bonds of silicon and oxygen are healed, and the film becomes compacted. When the annealing temperature exceeds 500 °C–600 °C, amorphous Si nanoinclusions are formed and then enlarged, with subsequent crystallization occurring at temperatures above 1000 °C. These structural transformations in the SiO_x layers lead to the observed changes in their optical properties, which are studied in detail in this paper.

2. Materials and methods

SiO_x films with a ~0.5 μm thickness were simultaneously deposited at a rate of 8 nm/s on ten 10 × 10 × 1 mm polished fused quartz substrates heated to T_d = 100 °C by thermal evaporation of 99.9% pure silicon monoxide SiO powder (Cerac Inc., Milwaukee, WI, USA) in vacuum at a residual pressure of (1–2) × 10^{-5} Torr. The deposition rate and thickness of the deposited films were controlled using a quartz-crystal microbalance thickness gauge (KIT-1) calibrated with an MII-4 micro-interferometer. The films were annealed for 15 min in a nitrogen atmosphere at temperatures T_{an} = 100 °C–1100 °C. The thicknesses of the resulting films were measured with an accuracy of ±5 nm using a LEF-3-M1 laser ellipsometer. The details of the used methodology can be found in the works [6,25].

The transmission T and reflection R spectra of these samples before and after annealing were measured in the wavelength range λ = 400–750 nm (photon energy $h\nu$ = 1.65–3.10 eV) using an apparatus based on the MDR-23 diffraction monochromator. The stoichiometry index x of the deposited films was evaluated using infrared spectroscopy performed on films deposited in the same vacuum cycle on double-polished silicon wafers. The method for determining x using IR spectral measurements is described in [26]; for our samples, the value x = 1.3 was obtained.

3. Results and discussion

Figure 1 illustrates the spectral evolution of the absorptance, $A = (1 - R - T)$, both prior to and following the annealing. There is an increase in A from 0.014–0.12 at the long-wave edge of the measuring range to 0.84–0.92 at its short-wave edge. The difference between A and 1 at the short-wave edge of the range is almost entirely due to the value of R, i.e., there is almost no transmission here. **Figure 1** also shows that the growth of T_{an} in the range 300 °C–500 °C gradually shifts the absorption edge to shorter wavelengths. However, annealing at 600 °C changes the direction of the absorption edge shift to the opposite. The long-wavelength shift in the absorption edge is augmented by annealing at 770 °C and is further enhanced by annealing at 910 °C. Annealing at 1010 °C shifts the absorption edge of the film to the short-wavelength side compared to annealing at 910 °C. Further increase in the annealing temperature to 1100 °C results in a shift of the absorption edge to a position that is in close proximity to that of the as-deposited film. Such a non-monotonic excursion of the absorption band edge indicates the complex nature of the structural changes undergone by the film during annealing. This is also evident in the shape of the absorption curves, which differs significantly for different annealing temperatures.

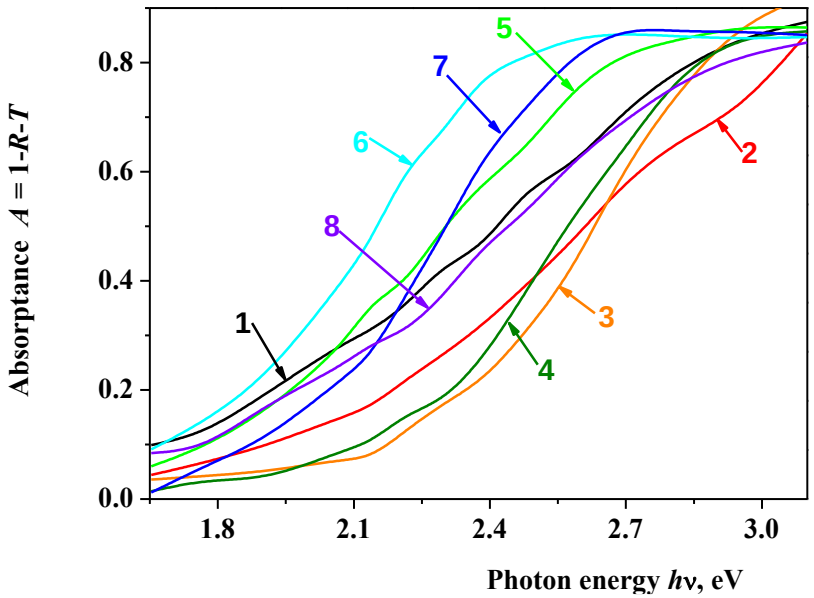

Figure 1. Absorptance spectra of $A = 1 - R - T$ of the as-deposited SiO_x film (1) and after 15-minute annealing at 300 (2), 500 (3), 600 (4), 770 (5), 910 (6), 1010 (7), and 1100 °C (8).

The absorption coefficient α of the films was determined by the formula [27]:

$$\alpha = \frac{1}{d} \ln \frac{T_s(1-R)}{T} \quad (1)$$

where T_s is the transmittance of the substrate without film. In amorphous, disordered, heterogeneous, nanostructured semiconductor and dielectric materials, there are usually regions of the spectra described by the Urbach dependence [28]:

$$\alpha(h\nu) = A \cdot \exp\left(h\nu / E_U\right) \quad (2)$$

The absorption in the region described by Equation (2) is caused by the superposition of transitions from localized states in the valence band tail to non-localized states in the conduction band and transitions from non-localized states in the valence band to localized states in the conduction band tail. In Equation (2), A is a numerical constant and E_U (Urbach energy) characterizes the width of the exponential absorption tail. It correlates with the widths of the tails of the localized valence band states γ_v and conduction band states γ_c and is mainly determined by the larger of the two, i.e., $E_U \sim \mathrm{Max}(\gamma_c, \gamma_v)$ [29].

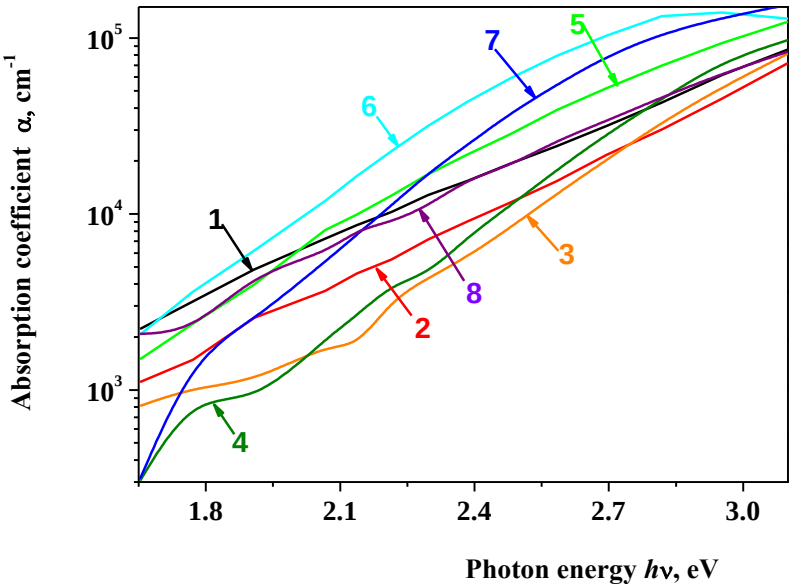

Figure 2. Spectra of the absorption coefficient α of the as-deposited SiO_x film (1) and after 15-minute annealing at 300 (2), 500 (3), 600 (4), 770 (5), 910 (6), 1010 (7), and 1100 °C (8), plotted in semi-logarithmic coordinates.

Figure 2 presents the absorption coefficient spectra plotted in semi-logarithmic coordinates. The relative error of the α values is 2%, which is only slightly greater than the thickness of the lines in the figure. As can be seen, the exponential dependence of the absorption coefficient on the photon energy in the as-deposited film and in the one annealed at 300 °C and 400 °C is quite well fulfilled in a significant part of the measured spectral range, including its high-energy edge. That is, this dependence is still observed at α values up to 8.46×10^4 cm^{-1} for the as-deposited film, 7.05×10^4 cm^{-1} after annealing at 300 °C. The corresponding E_U values were 0.42, 0.35 eV. After annealing at 500 °C and 600 °C, the Urbach region extends to 2.8 eV, with $\alpha \leq 3.3 \times 10^4$ and 5×10^4 cm^{-1}, respectively. E_U continues to decrease, reaching 0.26 and 0.23 eV, respectively. After annealing at 770 °C the corridor of fulfillment of the Urbach dependence narrows much more significantly both in terms of photon energy (to 2.1 eV) and absorption coefficient ($\alpha \leq 1.0 \times 10^4$ cm^{-1}), however, no further decrease in E_U is observed (E_U = 0.245 eV). The value of E_U after annealing at 910 °C is almost the same as that after annealing at 770 °C, but the straight-line section in semi-logarithmic coordinates extends to 2.4 eV ($\alpha \leq 4.3 \times 10^4$ cm^{-1}). The spectral range of the Urbach dependence and the value of the Urbach energy after annealing at 1010 °C are similar: $h\nu \leq 2.48$ eV, $\alpha \leq 3.7 \times 10^4$ cm^{-1}, E_U = 0.22 eV. After annealing at 1100

°C, the region of fulfillment of the Urbach dependence extends to 2.7 eV, with $\alpha \leq 3.4 \times 10^4$ cm^{-1}, E_U = 0.36 eV.

Thus, the absorption behavior in this deposited film, which is an alloy of silicon with oxygen, differs significantly from the behavior of amorphous homogeneous stoichiometric materials. First, in such materials, the Urbach dependence is observed at $\alpha < 10^4$ cm^{-1}. Secondly, the Urbach energy values themselves are much smaller. For example, in high-quality amorphous silicon films E_U = 0.042 eV [28], and in pure silica glass E_U = 0.075 eV [30].

For amorphous and composite materials, whose energy structure is characterized by the presence of localized states in the band gap (and, accordingly, the "blurring" of the valence band top and the conduction band bottom), several methods for determining the band gap width are used in the literature. For SiO_x, the formula proposed by Tauc et al. [31] is most widely used:

$$\alpha(E) = B \cdot (h\nu - E_o)^2/h\nu \quad (3)$$

In Equation (3), B is a numerical constant, and E_o is the Tauc optical band gap. Equation (3) describes the absorption due to indirect allowed transitions from non-localized states in the valence band to non-localized states in the conduction band. This postulates a quadratic dispersion law in both bands and the independence of the matrix element of optical transitions from the photon energy.

Figure 3 shows the absorption coefficient spectra plotted in the Tauc coordinates $h\nu - (\alpha \cdot h\nu)^{1/2}$. The Tauc optical bandgap E_o has been defined as the intersection of the linear approximation of the values of $(\alpha \cdot h\nu)^{1/2}$ in the high energy part of the spectrum with the abscissa. Comparing **Figures 2** and **3**, it is easy to see that the less the exponential dependence region extends into the high energy region, the further the observed Tauc dependence region extends into the low energy region. Although the Urbach energy E_U is almost halved by annealing, it is still at least three times higher than the Urbach energy in perfect SiO_2. This indicates a much greater structural disorder (which may also imply nanoheterogeneity) of these films both before and after annealing compared to the structure of amorphous silica in glassy form. Such large E_U values and the length of the exponential region up to $\alpha \geq 10^4$ cm^{-1} indicate that the Urbachian edge and interband transitions of different (nano)regions may overlap in these samples. In general, for a heterogeneous medium, the E_U and E_o values should be considered effective, since the heterogeneous medium differs in its structure from the "classical" amorphous medium.

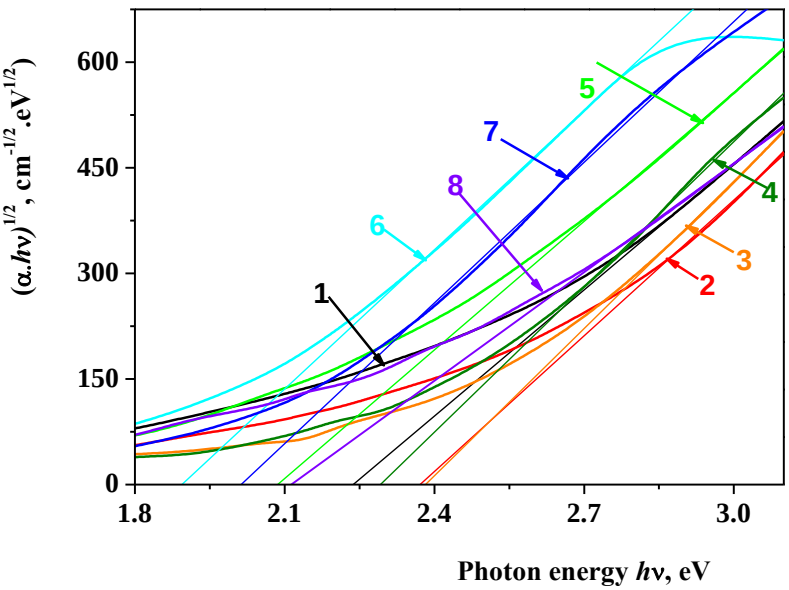

Figure 3. Spectra of the absorption coefficient α of the as-deposited SiO_x film (1) and after annealing for 15 min at 300 (2), 500 (3), 600 (4), 770 (5), 910 (6), 1010 (7), and 1100 °C (8), plotted in Tauc coordinates $h\nu - (\alpha \cdot h\nu)^{1/2}$.

Given the uncertainty involved in determining E_o, Tauc et al. [31] considered E_o to be an empirical quantity. In view of this, an alternative empirical measure of the optical band gap for amorphous semiconductors has been proposed: the isoabsorption band gap E_α. It corresponds to the photon energy at which the absorption coefficient α is equal to a specific value [32,33]. By analyzing the absorption spectra of *a*-SiH_x films with different degrees of disorder achieved by different degrees of hydrogenation, Cody et al. [34] found a linear anticorrelation between the optical band gap E_o and E_U in amorphous silicon:

$$E_o = E_g - C_o \cdot E_U \quad (4)$$

where E_g is the optical band gap limit at zero width of the tails of localized states (mobility gap). From the approximation Equation (4), a value of E_g ~ 2.1 eV was obtained with a constant C_o of 6.2. Thus, for defect-free amorphous silicon, the mobility gap is about 1 eV larger than for pure crystalline silicon. Grein and Johnn [35] found that the linear anticorrelation between E_o and E_U also occurs for *a*-As_2S_3 and *a*-As_2Se_3. A linear anticorrelation between E_α and E_U was observed for amorphous Ge in [33]. In this case, the approximation used to estimate the mobility band gap E_g was:

$$E_\alpha = E_g - C_\alpha \cdot E_U \quad (5)$$

It is expected that linear anticorrelations of the type Equations (4) and (5) will be fulfilled for a wide range of amorphous and disordered semiconductors.

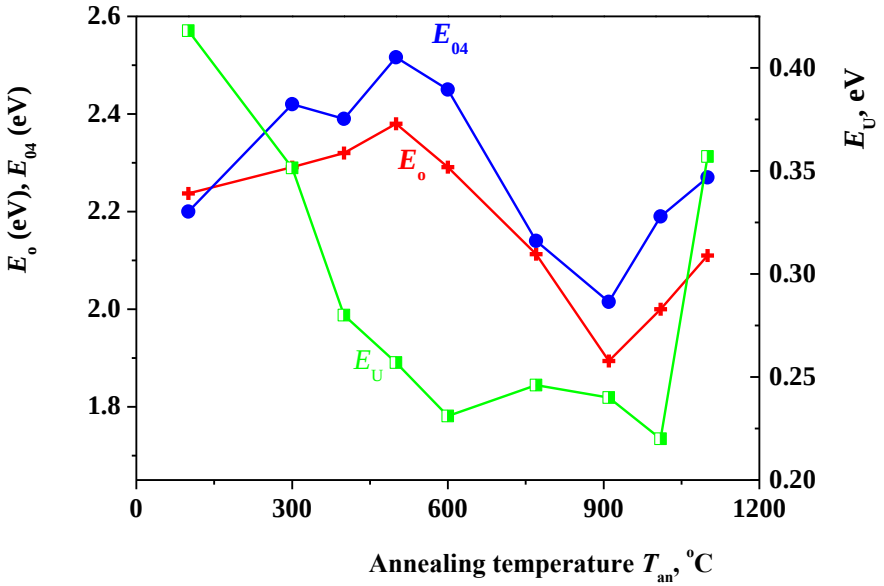

Figure 4. Dependence of the Urbach energy E_U, Tauc optical band gap E_o, and E_{04}—the isoabsorption band gap at $\alpha = 10^4$ cm^{-1}—on the annealing temperature of the $SiO_{1.3}$ film in a nitrogen atmosphere for 15 min.

Figure 4 shows the temperature dependence of E_{04}, E_o, and E_U for the investigated samples. The isoabsorption band gap E_{04} corresponds to the photon energy at which $\alpha = 10^4$ cm^{-1}. The error in determining the obtained values of E_U, E_o and E_{04} in our case was ±0.01 eV. Different temperature regions can be distinguished in these dependences. First, there is a clear anti-correlation between the value of E_U, on the one hand, and the values of E_{04} and E_o, on the other hand, at annealing temperatures $T_{an} \leq 500$ °C. By analogy with the results of the above works, it is logical to assume that changes in the parameters E_{04}, E_o, and E_U in the range of annealing temperatures up to 500 °C are due to a decrease in the degree of structural disorder of the film with increasing T_{an}. The linear approximation of the $E_{04}(E_U)$ dependence in this annealing temperature range gave the $E_g = E_{04}(E_U = 0) = 3.00 \pm 0.16$ eV, and the linear approximation of the $E_o(E_U)$ dependence gave the value $E_g = E_o(E_U = 0) = 2.63 \pm 0.13$ eV. Based on these results, the mobility gap E_g of amorphous $SiO_{1.3}$ can be estimated to be $E_g = 2.50$–3.16 eV. In [36], the value of E_g for SiO_x alloys in the bulk glassy state was calculated using density functional theory. These calculations gave a value of $E_g = 2.5$ eV for $x = 1.3$. Although this value, as the authors point out, is an underestimate due to the peculiarities of the method, it correlates better with the E_g value obtained using the Tauc optical band gap.

With an increase in T_{an} from 500 °C to 600 °C and further to 910 °C a significant decrease in the values of E_{04} and E_o is observed compared to their values at T_{an} = 500 °C. This takes place against the background of a slight decrease in the value of the E_U. This shows that, at these annealing temperatures, the prevailing processes are fundamentally different from the processes of structural ordering of the $SiO_{1.3}$ film that take place at $T_{an} \leq 500$ °C. It is known that, at high annealing temperatures, SiO_x films undergo disproportionation with the formation of amorphous [21,37–40], and, at $T_a \geq$ 800 °C–900 °C, amorphous, amorphous-crystalline, and crystalline silicon nanoinclusions [37–40] in the matrix of the SiO_y ($y > x$) composition. In suboxide SiO_x

films with stoichiometry indices $x \leq 1.5$, the optical band gap E_o grows very rapidly with increasing x [3]. Thus, the main contribution to the absorption of the nanocomposite 'Si nanoinclusions—SiO_y' after annealing at 600 °C ≤ T_{an} ≤ 800 °C–900 °C should be attributed to the amorphous silicon nanoparticles. As can be seen from the graph, they already begin to play a noticeable role at T_{an} = 600 °C. The decrease in the values of the empirical parameters E_{04} and E_o with further growth of T_{an} can, obviously, be interpreted as a manifestation of the size effect in amorphous silicon nanoparticles.

The E_U values for annealing temperatures of 600 °C–910 °C do not demonstrate any pronounced trend depending on the sizes of amorphous inclusions: The E_U almost does not change, remaining at the level of values slightly lower than after annealing at 500 °C. This distinguishes the behavior of the '*a*-Si nanoinclusions—SiO_y' ($y > 1.3$) nanocomposites from the behavior of the '*c*-Si nanoinclusions—SiO_2' nanocomposites. The latter are characterized by the growth of the E_U with decreasing nanocrystallite size due to the increasing influence of the c-Si/SiO_2 interface [41]. The values of E_U = 0.23–0.246 eV obtained by us in this range of annealing temperatures are very close to the values of E_U obtained in [42] for non-hydrogenated *a*-Si films with thicknesses of 769–1174 nm, grain sizes of 20–30 nm, and porosities of 0.14–0.24 (i.e., with natural oxide-coated grains). The E_U values in these films were 0.230–0.258 eV, and the E_o values were 1.32–1.38 eV. Almost identical E_U values and higher E_o values for the nanocomposite films '*a*-Si nanoinclusions—SiO_y' obtained by annealing $SiO_{1.3}$ films at temperatures of 600 °C–910 °C compared to the non-hydrogenated *a*-Si films can be explained by the size effect. It causes an increase in the band gap of amorphous silicon inclusions with decreasing size.

If we assume that for the non-hydrogenated partially porous oxidized *a*-Si films there is the anticorrelation (Equation 4) with the same coefficient C_o = 6.2, then we obtain a mobility gap $E_g \sim 2.8$ eV. Assuming the validity of Equation (4) with C_o = 6.2 for the $SiO_{1.3}$ films annealed at 600 °C–910 °C, we obtain estimates of the mobility gap $E_g \approx 3.4$–3.75 eV. If we assume that E_g for non-hydrogenated partially porous oxidized *a*-Si films is the same as for hydrogenated films, i.e., 2.1 eV, and that for them Equation (4) is fulfilled, then the coefficient of such an anticorrelation is C_o = 3.0. If we accept this coefficient for the films obtained by annealing $SiO_{1.3}$ films at 600 °C–910 °C, we obtain an estimate of the mobility gap $E_g \approx 2.61$–2.98 eV. In [43], the values of E_o were determined for non-hydrogenated a-Si nanoparticles (nanodots) in a solution of highly purified ethanol. Unfortunately, the authors did not determine the value of E_U in their samples. Therefore, the obtained values of the optical band gap E_o, which increased from 2.58 eV for particles with an average diameter of 5.15 nm to 3.22 eV for particles with an average diameter of 1.15 nm, are lower estimates of E_g. As can be seen, these estimates of E_g for nanoparticles in ethanol are still in better agreement with the estimates of E_g for nanoparticles in our suboxide matrix at a value of the coefficient C_o = 3.0 in Equation (4), which is not surprising.

The application of annealing at 1010 °C in comparison to annealing at 910 °C has been observed to result in an increase in E_{04} and E_o, while E_U exhibited a decrease from 0.24 to 0.22 eV. In works [44,45] the nucleation of crystalline inclusions in amorphous *a*-Si:H films was studied using the Tauc-Lorentz parametric model. It was

determined that this results in an increase in the optical (Tauc) band gap E_o and a decrease in the parameter Γ (half-width of the Lorentz oscillator function), which serves as a measure of the film disorder. These results provide a rationale for associating the observed increase in E_o and decrease in E_U following annealing at 1010 °C with an increase in the ordering of the amorphous nanoparticles' structure, including the formation of a quasi-crystalline core.

Annealing at 1100 °C maintains the tendency of increasing E_{04}, E_o. The value of E_o = 2.11 eV is very close to the value of E_o = 2.1 eV for the $SiO_{1.3}$ film obtained by molecular beam deposition after its annealing at 1100 °C [46]. After such annealing, the film contains both crystalline and amorphous nanoparticles, and E_o should be considered as the effective (averaged) optical band gap. Following annealing at 1100 °C, a pronounced increase in E_U for our film is observed, which is indicative of the presence of silicon nanoparticles exhibiting diverse structural and size characteristics. In their investigation of 'silicon nanocrystallites—SiO_2' superlattices, the authors [41] identified a direct correlation between the concentration of so-called P_b centers—dangling bonds of silicon atoms at the Si/SiO_2 boundary—and the Urbach energy, E_U. Given that the appearance of P_b centers was recorded following annealing of the films with a similar composition to ours at 1100 °C [37], it is reasonable to conclude that the formation of these centers also contributes to the observed increase in E_U.

4. Conclusion

Non-stoichiometric SiO_x ($x \approx 1.3$) films exhibit significant variations in the behavior of the fundamental absorption edge as a function of the annealing temperature. At annealing temperatures $T_a \leq 500$ °C, a short-wavelength shift of the absorption edge occurs, which is then replaced by a long-wavelength shift in the range 600 °C $\leq T_a \leq$ 900 °C. The short-wavelength shift is accompanied by an increase in the optical band gap E_o and a decrease in the Urbach energy E_U, indicating structural ordering of the film. In this case, defect annealing, healing of broken silicon and oxygen bonds, film densification, and a corresponding decrease in defect absorption take place. The long-wavelength shift is due to film disproportionation and the formation of amorphous silicon inclusions, which exhibit significant indirect interband absorption. E_o decreases with increasing amorphous silicon nanoparticle size and their volume fraction in the annealed film, while E_U remains almost unchanged. By further increasing the annealing temperature of the SiO_x film, the absorption edge shifts to shorter wavelengths again, and both E_o and E_U increase. The increase in E_o in this case is due to the increasing fraction of the crystalline silicon phase (c-Si nanocrystals have a larger band gap) and a decrease in the fraction of amorphous silicon, while the increase in E_U is attributed to the corresponding increase in the area of the c-Si/SiO_2 interface, where interface centers (P_b centers) form.

Author contributions: Conceptualization, MS and II; methodology, MS, II and VY; validation, II and KM; investigation, II, VY and MS; writing—original draft preparation, MS and KM; writing—review and editing, MS, II, KM and VY;

visualization, KM; supervision, II. All authors have read and agreed to the published version of the manuscript.

Acknowledgments: The authors would like to thank Jeffrey Monastyrsky (USA) for his help with the English edition of this article.

Institutional review board statement: Not applicable.

Informed consent statement: Not applicable.

Dedication: This article is dedicated to the memory of our colleague and friend, Dr Petro Shepeliavyi, who recently passed away. He was a prolific author of many sophisticated technological developments that significantly advanced both fundamental research and the creation of specific devices. Among his notable contributions are developments utilizing SiO_x films and structures based on them. These include the development of technologies for manufacturing solid and porous light-emitting silicon–silicon oxide nanocomposites, light-sensitive $SiO\text{-}As_2(S,Se)_3$ nano multilayers, gradient light-absorbing SiO_x/Me coatings for display panels, thin film SiO_x<Ti>, SiO_x<Fe> nanocomposites combining functions of IR-absorption and formation of an electric signal for the thermosensitive detectors operating in γ-radiation fields.

Conflict of interest: The authors declare no conflict of interest.

References

1. Savage JA. Infrared Optical Materials and their Antireflection Coatings. Bristol: Adam Higler Ltd; 1985.
2. Wetch KW. Large-range refractive-index control of silicon monoxide antireflection coatings using oblique incident thermal evaporation. Applied Optics. 1991; 30(28): 4133. doi: 10.1364/ao.30.004133
3. Tomozeiu N. Silicon Oxide (SiO_x, 0< x < 2): a Challenging Material for Optoelectronics. In: Predeep P (editor). Optoelectronics: Materials and Techniques. IntechOpen; 2011. pp. 55–98.
4. Melnik VP, Popov VG, Romanyuk BM, et al. Luminescent properties of the structures with embedded silicon nanoclusters: Influence of technology, doping and annealing (Review). Semiconductor Physics, Quantum Electronics & Optoelectronics. 2023; 26(3): 278–302. doi: 10.15407/spqeo26.03.278
5. Falcony C, Estrada-Wiese D, De Anda J, et al. Low temperature (<700 °C) SiO_2 and Si-rich SiO_2 films: Short review. Journal of Vacuum Science & Technology B. 2023; 41(3). doi: 10.1116/6.0002531
6. Sopinskyy MV, Vlasenko, NA, Lisovskyy IP, et al. Formation of nanocomposites by oxidizing annealing of SiO_x and SiO_x <Er,F> films: Ellipsometry and FTIR analysis. Nanoscale Research Letters. 2015; 10(1). doi: 10.1186/s11671-015-0933-0
7. Michailovska K, Indutnyi I, Shepeliavyi P, et al. The effect of fluorine–hydrogen treatment on the photoluminescent properties of multilayer $(nc\text{-}Si–SiO_x–SiO_y)_n$ nanostructures with porous barrier layers. Applied Nanoscience. 2020; 10(12): 4695-4701. doi: 10.1007/s13204-020-01404-z
8. Michailovska, KV, Indutnyi, IZ, Shepeliavyi, PE, et al. Formation of silicon nanocomposites by annealing of $(SiO_x/Sm)_n$ multilayers: luminescence, Raman and FTIR studies. Applied Nanoscience. 2023; 13(11): 7187-7194. doi: 10.1007/s13204-023-02887-2
9. Sarikov A. Thermodynamic theory of phase separation in nonstoichiometric Si oxide films induced by high-temperature anneals. Nanomanufacturing. 2023; 3(3): 293–314. doi: 10.3390/nanomanufacturing3030019
10. Nayfeh MH. Fundamentals and Applications of Nano Silicon in Plasmonics and Fullerines: Current and Future Trends. Elsevier Publishing, Cambridge, MA; 2018.
11. Khriachtchev L. Silicon Nanophotonics: Basic Principles, Present Status, and Perspectives. Pan Stanford Publishing; 2016.
12. Yuan Z, Anopchenko A, Pavesi L. Innovative quantum effects in silicon for photovoltaic applications. In: Pizzini S (editor). Advanced Silicon Materials for Photovoltaic Applications. John Wiley & Sons; 2012. pp. 355–391. doi: 10.1002/9781118312193.ch10

13. Sopinskyy M, Khomchenko V. Electroluminescence in SiO_x films and SiO_x film-based systems. Curr Opin Solid State Mater Sci. 2003; 7(2): 97–109. doi: 10.1016/S1359-0286(03)00048-2
14. Bratus' OL, Evtukh AA, Ievtukh A, et al. Nanocomposite SiO_2(Si) films as a medium for non-volatile memory. Journal of Non-Crystalline Solids. 2008; 354(35-39): 4278-4281. doi: 10.1016/j.jnoncrysol.2008.06.037
15. Shieh JM, Lai YF, Ni WX, et al. Enhanced photoresponse of a metal-oxide semiconductor photodetector with silicon nanocrystals embedded in the oxide layer. Applied Physics Letters. 2007; 90(5). doi: 10.1063/1.2450653
16. Evtukh AA, Litovchenko VG, Semenenko MO. Electrical and emission properties of nanocomposite SiO_x(Si) and SiO_2(Si) films. Journal of Vacuum Science & Technology B: Microelectronics and Nanometer Structures Processing, Measurement, and Phenomena. 2006; 24(2): 945-949. doi: 10.1116/1.2183787
17. Yao J, Sun Z, Zhong L, et al. Resistive switches and memories from silicon oxide. Nano Letters. 2010; 10(10): 4105-4110. doi: 10.1021/nl102255r
18. Mehonic A, Shluger AL, Gao D, et al. Silicon oxide (SiO_x): A promising material for resistance switching? Advanced Materials. 2018; 30(43). doi: 10.1002/adma.201801187
19. Chen W, Fang R, Balaban MB, et al. A CMOS-compatible electronic synapse device based on Cu/SiO_2/W programmable metallization cells. Nanotechnology. 2016; 27(25): 255202. doi: 10.1088/0957-4484/27/25/255202
20. Ugwumadu C, Subedi KN, Thapa R, et al. Structure, vibrations and electronic transport in silicon suboxides: Application to physical unclonable functions. Journal of Non-Crystalline Solids: X. 2023; 18: 100179. doi: 10.1016/j.nocx.2023.100179
21. Lisovskyy IP, Indutnyy IZ, Gnennyy BN, et al. Structural-phase transformations in SiO_x films in the course of vacuum heat treatment. Semiconductors. 2003; 37(1): 97–102. doi: org/10.1134/1.1538546
22. Zacharias M, Heitmann J, Scholz R, et al. Size-controlled highly luminescent silicon nanocrystals: A SiO/ SiO_2 superlattice approach. Applied Physics Letters. 2002; 80(4): 661-663. doi: 10.1063/1.1433906
23. Szekeres A, Nikolova T, Paneva A, et al. Silicon clusters in silicon monoxide films. Journal of Optoelectronics and Advanced Materials. 2005; 7(3): 1383–1387.
24. Garrido Fernandez B, Lopez M, Garcıa C, et al. Influence of average size and interface passivation on the spectral emission of Si nanocrystals embedded in SiO_2. Journal of Applied Physics. 2002; 91(2): 798-807. doi: 10.1063/1.1423768
25. Sopinskii NV, Khomchenko VS, Litvin OS, et al. Properties of low-refractive-index films obtained by the close-spaced vapor transport technique under the sublimation of graphite in a quasi-closed volume. Technical Physics. 2011; 56(11): 1665-1669. doi: 10.1134/s1063784211110259
26. Nakamura M, Mochizuki Y, Usami K, et al. Infrared absorption spectra and compositions of evaporated silicon oxides (SiO_x). Sol St Commun. 1984; 50(12): 1079–1081. doi: 10.1016/0038-1098(84)90292-8
27. Raciti R, Bahariqushchi R, Summonte C, et al. Optical bandgap of semiconductor nanostructures: Methods for experimental data analysis. Journal of Applied Physics. 2017; 121(23). doi: 10.1063/1.4986436
28. Cody GD. Urbach edge of crystalline and amorphous silicon: a personal review. J. Non-Cryst. Solids. 1992; 141: 3–15. doi: 10.1016/S0022-3093(05)80513-7
29. O'Leary SK, Johnson SR, Lim PK. The relationship between the distribution of electronic states and the optical absorption spectrum of an amorphous semiconductor: An empirical analysis. Journal of Applied Physics. 1997; 82(7): 3334-3340. doi: 10.1063/1.365643
30. Saito K, Ikushima AJ. Absorption edge in silica glass. Physical Review B. 2000; 62(13): 8584-8587. doi: 10.1103/physrevb.62.8584
31. Tauc J, Grigorovici R, Vancu A. Optical properties and electronic structure of amorphous germanium. Phys. Status Solidi B. 1966; 15(2): 627–637. doi: 10.1002/pssb.19660150224
32. Freeman EC, William P. Optical constants of rf sputtered hydrogenated amorphous Si. Physical Review B. 1979; 20(2): 716-728. doi: 10.1103/physrevb.20.716
33. Persans PD, Ruppert AF, Chan SS, et al. Relationship between bond angle disorder and the optical edge of a-Ge:H. Solid State Commun. 1984; 51(4): 203–207. doi: 10.1016/0038-1098(84)90996-7
34. Cody GD, Tiedje T, Abeles B, et al. Disorder and the optical-absorption edge of hydrogenated amorphous silicon. Physical Review Letters. 1981; 47(20): 1480-1483. doi: 10.1103/physrevlett.47.1480
35. Grein CH, John S. Temperature dependence of the Urbach optical absorption edge: A theory of multiple phonon absorption and emission sidebands. Physical Review B. 1989; 39(2): 1140-1151. doi: 10.1103/physrevb.39.1140

36. Bondi RJ, Lee S, Hwang GS. First-principles study of the mechanical and optical properties of amorphous hydrogenated silicon and silicon-rich silicon oxide. Physical Review B. 2010; 81(19). doi: 10.1103/physrevb.81.195207
37. Bratus' VY, Yukhimchuk VA, Berezhinsky LI, et al. Structural transformations and silicon nanocrystallite formation in SiO_x films. Semiconductors. 2001; 35(7): 821–826. doi: 10.1134/1.1385719
38. Nikolenko AS, Sopinskyy MV, Strelchuk VV, et al. Raman study of Si nanoparticles formation in the annealed SiO_x and SiO_x:Er,F films on sapphire substrate. J Optoelectron Adv Mater. 2012; 14(1–2): 120–124.
39. Sarikov A. Crystallization behaviour of amorphous Si nanoinclusions embedded in silicon oxide matrix. Phys. Status Solidi A. 2019; 217(4): 1900513. doi: org/10.1002/pssa.201900513
40. Lisovskyy IP, Voitovich MV, Sarikov AV, et al. Transformation of the structure of silicon oxide during the formation of Si nanoinclusions under thermal annealings. Ukr J Phys. 2009; 54(4): 383–390.
41. Lee BG, Hiller D, Luo JW, et al. Strained interface defects in silicon nanocrystals. Advanced Functional Materials. 2012; 22(15): 3223-3232. doi: 10.1002/adfm.201200572
42. Ballester M, Márquez AP, García-Vázquez C, et al. Energy-band-structure calculation by below-band-gap spectrophotometry in thin layers of non-crystalline semiconductors: A case study of unhydrogenated a-Si. Journal of Non-Crystalline Solids. 2022; 594: 121803. doi: 10.1016/j.jnoncrysol.2022.121803
43. Askari S, Svrcek V, Maguire P, et al. The interplay of quantum confinement and hydrogenation in amorphous silicon quantum dots. Advanced Materials. 2015; 27(48): 8011-8016. doi: 10.1002/adma.201503013
44. Collins RW, Koh J, Ferlauto AS, et al. Real time analysis of amorphous and microcrystalline silicon film growth by multichannel ellipsometry. Thin Solid Films. 2000; 364(1–2): 129–137. doi: 10.1016/S0040-6090(99)00925-6
45. Abdulraheem Y, Gordon I, Bearda T, et al. Optical bandgap of ultra-thin amorphous silicon films deposited on crystalline silicon by PECVD. AIP Advances. 2014; 4(5): 057122. doi:10.1063/1.4879807
46. Nikitin T, Velagapudi R, Sainio J, et al. Optical and structural properties of SiO_x films grown by molecular beam deposition: Effect of the Si concentration and annealing temperature. Journal of Applied Physics. 2012; 112(9). doi: 10.1063/1.4764893